

# The Momentum Matrix method and its use for the modelling of semiconductor superlattices in electric and magnetic fields

T. A. Vaughan<sup>1</sup>, A. J. L. Poulter<sup>2</sup>, R. J. Nicholas, C. C. Chang

*Physics Department, Oxford University, Clarendon Laboratory, Parks Road, Oxford, OX1 3PU,*

*U. K.*

## Abstract

We present a procedure to solve  $k,p$  theory for semiconductor heterostructures using the envelope function approximation solved in momentum space. The technique which we term the momentum matrix method, solves the band structure of semiconductor superlattices very efficiently by transforming the Hamiltonian and electric potentials into  $k$ -space. The method also successfully tackles the spurious solution problem appearing through the incompleteness of the Hamiltonian. We outline the theory behind this procedure and demonstrate the ability of the method to model a variety of heterostructure phenomena including self-consistency, perpendicular magnetic field, electric fields and doping. The method shows substantial advantages over other non-self consistent models in Type-II crossed gap systems where the definition of charge density is not straightforward.

<sup>1</sup> Current address: Microsoft Corporation, Seattle, U.S.A.

<sup>2</sup> Current address: CNRS-MPI, 25 Avenue des Martyrs, BP 166, Grenoble, Cedex 9, France.

## I. Introduction

**K.p** theory was first constructed over forty years ago to explain cyclotron resonance in bulk materials [1,2]. Since then it has been applied to numerous materials, both bulk and heterostructures [3-6] and is widely used today for the design of opto-electronic and electrical devices [7-8]. Although **k.p** theory was initially developed for bulk materials, it has been successfully extended to model heterostructures using the envelope function approximation (EFA) [9-10]. A number of different methods are used within the EFA to solve the band structure the most common being the transfer-matrix [11-13], finite difference [14], finite element[15], and scattering matrix [16] techniques. These methods however suffer a number of complications when applied to heterostructures; firstly the problem of matching envelope functions at the interface is still not completely resolved, and is a source of continued debate [16-18]; and secondly the techniques in their simplest forms are limited to flat band potentials, thus limiting the modelling of charge transfer, electric fields and doping. This second point can be overcome by using a mesh technique where the layers are split into a number of sub-layers with the band potential varying between sub-layers. Furthermore the commonly used transfer-matrix technique is beset by the problem of spurious solutions which relates to the solutions whose wavevectors exist well outside the first Brillouin zone. Although the spurious solutions relate to unphysical states and can lead to numerical problems or spurious energy solutions [19], they cannot simply be dropped as they influence the physical states of the structure. Although methods have been developed to try and overcome these problems, the above techniques are still only suited to thin-layer structures with flat or nearly flat band potentials. Alternatively one can move to approaches based on the use of pseudopotentials which overcome many of the

fundamental problems of an EFA [20] but which are still quite computationally demanding and give less relative accuracy.

In this paper we build on the work of Winkler and Rossler [21] who showed how the EFA can be successfully transformed into momentum space, thus avoiding the problems explained above. The previous work is extended here to model superlattices, and we show how a general model can be designed so as to calculate the band structure of any III/V semiconductor heterostructure (single heterostructure, quantum well or superlattice), with an arbitrary layer sequence and doping profile. The technique, which we term the Momentum Matrix Method (MMM) is then extended to include the effects of band occupation and charge transfer using a self-consistent routine. In most of the work described here we use the MMM to model the crossed gap system InAs/GaSb. In such a case the definition of the self-consistent potential is non-trivial, and cannot be simply related to an integration over electron (hole) states below (above) the Fermi level as one would perform in a wide gap Type I heterostructure. We discuss this final point in detail as there is a lack of material and some misunderstanding on this subject in the literature.

## **II. The momentum matrix method**

The use of  $\mathbf{k}\cdot\mathbf{p}$  theory to model the band structure of bulk material is hugely simplified by considering the symmetry of the lattice. A carrier moving through the structure sees an infinite number of nuclear cores at defined lattice sites, such that the structure of lattice sites surrounding a particular site can be simply related to the structure surrounding any other site using defined symmetry operations. This periodicity however is broken in heterostructures, as different layers of material alter the form of the crystal lattice in different locations. The method commonly used

to overcome these difficulties is the envelope function approximation (EFA) which we will briefly outline before detailing the MMM. For the development of the EFA we consider the case of a simple binary superlattice consisting of alternating layers of two bulk materials  $A$  and  $B$  with widths  $d_1$  and  $d_2$ , respectively (Fig. 1). The materials  $A$  and  $B$  are III-V or II-VI semiconductors with a bulk band structure which is well described by the  $\mathbf{k}\cdot\mathbf{p}$  Hamiltonian, having conduction and valence bands with band edges with  $\Gamma_6$ ,  $\Gamma_7$  and  $\Gamma_8$  symmetry properties. We consider an eight band description of the band structure including the  $J = 3/2$  heavy hole and light hole bands along with the  $J = 1/2$  spin-orbit split off band and the  $J = 1/2$  conduction band states. The Kane basis states [1,3,4] that we use are shown in Table 1. In the EFA the modelling of superlattices is achieved by assuming that the wavefunction can be written as a linear superposition of the Kane basis states (as in the bulk case), which are modulated by a function which is slowly varying over the unit cells - called the envelope function. This is written as follows where we have taken the heterostructure confinement direction to lie parallel to the  $z$ -axis:

$$\psi(\mathbf{r}) = \sum_m^{\Gamma} F_m(z) \chi_m(x, y) |u_{m\Gamma}(\mathbf{r})\rangle$$

(1)

The general envelope function has been separated into an envelope function  $F_m(z)$  and as yet an unspecified function  $\chi_m(x, y)$  which modulates the wavefunction in the plane of the layers. In this paper we consider the band structure of superlattices and hence Equ. 1 is modified by the superlattice Bloch condition:

$$\psi(\mathbf{r}) = e^{iqz} \sum_m^{\Gamma} f_m(z) \chi_m(x, y) |u_{m\Gamma}(\mathbf{r})\rangle \quad (2)$$

with  $q$  taking values  $-\frac{\pi}{d} < q < \frac{\pi}{d}$ , where  $d=d_1+d_2$ . This in essence is the approximation used in the EFA – though the actual approximations contained within this are more complex [22]. Firstly this approximation assumes that the Kane basis states are identical in all layers, though calculations performed using different Kane basis states in each layer indicate that this assumption is valid for most materials [23]. Secondly the use of the same basis states in each layer removes any atomic information about the interface. To perform calculations that include such details, the states must be built from atomic orbitals [24-25].

To solve the band structure using the MMM, we construct a matrix which represents the evolution of the wavefunction in momentum space. The model contains the basic elements of pseudopotential techniques [26] and is an extension of the work of Winkler and Rössler [21] to superlattices. As well as being flexible with respect to band edge potentials and layer thickness, the method is also algorithmically compact, being fully described by only a few equations. The starting point for the MMM is to describe the wavefunctions in terms of the EFA as detailed above. The Schrodinger equation for the structure is simply:

$$\left(H^{A,B} + V^{A,B}\right) \varphi^{A,B}(\mathbf{r}) = E \varphi^{A,B}(\mathbf{r}) \quad (3)$$

where  $V^{A,B}$  is the offset between the bands in the constituent bulk materials. The bulk Hamiltonian matrix is separated into coefficients of the growth direction momentum operator  $k_z$ . A Hermitian form for these coefficients must be chosen, although there is no unique Hermitian formulation [27], we choose the form:

$$H\psi(\mathbf{r}) = \left[k_z H_2 k_z + \frac{1}{2}(H_1 k_z + k_z H_1) + H_0\right] \psi(\mathbf{r}) = E \psi(\mathbf{r}) \quad (4)$$

Instead of turning to real space to determine the propagation of the wavefunction through each material layer, the periodicity of the superlattice is exploited. The  $\mathbf{k}, \mathbf{p}$  Hamiltonian, potential and

envelope functions are periodic in real space with a periodicity of the superlattice period  $d$ , and thus can be represented by a summation over Fourier components:

$$\mathbf{G}_j = \frac{2\pi j}{d} \quad \text{where } j=0,1,2\dots FF \quad (5)$$

$FF$  is the number of Fourier components used in the calculation which is an important input parameter, the number of Fourier components required depending on the complexity of the structure that is being modelled. This will be discussed further later on. The only term in Equ. 4 that does not contain this periodicity is the superlattice Bloch term  $e^{iqz}$ , which is operated upon by the terms in the Hamiltonian. The Hamiltonian, potential and envelope functions can then be written as functions of the Fourier components of  $\mathbf{G}_j$ . Re-writing Equ. 4 in  $k$ -space yields the following equation, where the coefficients of the operator  $k_z$  represent the Fourier transform of the corresponding components in Equ. 4:

$$\{k_z H_2(z) k_z + \frac{1}{2} [H_1(z) k_z + k_z H_1(z)] + H_0(z) + V(z)\} f_m(z) = E_m f_m(z) \quad (6)$$

where:

$$H_i(z) = \sum_{j=0}^{FF} H_i^j e^{iG_j z} \quad V(z) = \sum_{j=0}^{FF} V^j e^{iG_j z} \quad f_m(z) = \sum_{j=0}^{FF} f_m^j e^{iG_j z}$$

$FF$  is the number of Fourier terms used and  $d$  is the superlattice period. It can then be shown that the Fourier coefficients of the Hamiltonian, potential and envelope function are related by:

$$\sum_k \left( (q + G_j)(q + G_k) H_2^{j-k} + (q + \frac{1}{2}(G_j + G_k)) H_1^{j-k} + H_0^{j-k} + V^{j-k} \right) \phi^k = E \phi^j \quad (7)$$

This can be re-written as a matrix eigenvalue equation:

$$\mathbf{M}(q)\mathbf{F} = E\mathbf{F} \quad (8)$$

The elements of eigenvalue  $\mathbf{F}$  are the Fourier coefficients of the envelope function  $f_m$  and the matrix  $\mathbf{M}(q)$  is defined:

$$M_{jk}(q) = (q + G_j)(q + G_k)H_2^{j-k} + (q + \frac{1}{2}(G_j + G_k))H_1^{j-k} + H_0^{j-k} + V^{j-k} \quad (9)$$

To obtain the electronic band structure of the superlattice at zero magnetic field the envelope function in the  $x$  and  $y$  directions is replaced by plane waves:  $\chi(x, y) = e^{ik_x x} e^{ik_y y}$ . The values of  $(k_{//}, q)$  at a given point are entered into the  $M(q)$  matrix which is then diagonalized. The eigenvalues of the matrix are the eigenenergies, and the corresponding eigenvectors are the Fourier coefficients of the envelope function. The total dimension of the  $M(q)$  matrix will be the dimension of the Hamiltonian, multiplied by the number of Fourier terms which can be of the order of 20-30 for the most complex structures. Thus for 8-band Hamiltonians the  $M(q)$  matrix can be as large as 240×240. Although this is much larger than the matrices in standard transfer matrix approaches (the matrix being twice the size of the Hamiltonian), the matrix is diagonalized only once per  $(k_{//}, q)$  point, with the accuracy of the eigenvalues determined solely by the number of Fourier terms used. For most of the work performed at zero magnetic field we have used a 4×4 Block diagonalization of the matrix [28] so as to reduce the computing time. In this Block diagonalization the warping parameter ( $\mu$ ) presents a problem (these non-symmetric terms cannot be Block diagonalized) and although Cohen treats this term as a perturbation we set  $\mu=0$  (known as the axial approximation). The errors in neglecting these terms are found to be small, only appearing at large values of  $k$  parallel [28]. By calculating the subband energies separately at each  $(k_{//}, q)$  point, the method does not directly evaluate the dispersion relations of quantum confined subbands, as in the transfer matrix approach. Thus in the above formulation the idea of a “subband” is not a well defined quantum number as in the Kronig-Penney model. Instead, a series of eigenvalues at each  $(k_{//}, q)$  value are found which are matched so as to form subbands.

A similar procedure is used to obtain the band structure at finite magnetic field. The envelope functions in the  $x$  and  $y$  directions are replaced by the harmonic oscillator wave functions, which account for the magnetic field quantisation of the states into Landau levels. To solve the structure in magnetic fields, one diagonalizes the Hamiltonian with magnetic field  $B$  and Landau level index  $n$  as input parameters. Since index  $n$  is actually the superposition of the spin and the in-plane angular momentum, not all the basis states necessarily contribute to the eigenstates due to the different spin the basis carries. We have followed the standard procedure to derive and determine the matrix at a given Landau level index [29]. In the magnetic field calculations a full  $8 \times 8$  matrix is used, as a block  $4 \times 4$  diagonalization is not appropriate.

For both cases the total wavefunction of a state can be expressed as:

$$\psi(\mathbf{r}) = e^{iqz} \sum_n^{\Gamma} \sum_{j=0}^{FF} \phi_n^j e^{iG_j z} \chi_n(x, y) |\Gamma_n\rangle$$

(10)

where  $\phi_n^j$  stands for the  $j^{\text{th}}$  Fourier term of the  $n^{\text{th}}$  Kane state.

An important point to consider is the number of Fourier terms used in a calculation, and how this affects the validity of the calculation. For most structures discussed in section IV of this paper the number of Fourier terms was quite small, set at 12 or less (the actual number is presented with each set of data in the section). For a general guide we consider that the minimum number of Fourier terms used should be  $\sim 8$ , and should also relate to the superlattice period such that:

$$FF \approx d / 25$$

The superlattice period  $d$  being in Angstroms. For the case of structures containing a mixture of very narrow and wide layers this number will need to be increased. However the small number

of Fourier terms that are used means that we are not calculating the superlattice zone folded bands, as the Fourier series is truncated well before the Brillouin zone boundary. Although this removes the problem of spurious solutions in this model, the truncation of the Fourier series affects the eigenstates far away from the superlattice band gap, limiting the energy range over which the model is applicable. Calculations have shown that the model is successful in accurately determining eigenstates which are confined by the heterostructure potential. The model becomes less accurate when determining un-confined bulk like states.

To show how the accuracy of the confined energy levels relates to the number of Fourier terms used in the calculation we have performed a series of calculations on the InAs/GaSb superlattice which is described further in section IV. The results are presented in Table 2. The calculations were performed self-consistently (self-consistency is described in detail in the next section) and the only parameter that differed between them was the number of Fourier terms. It can be seen that even with only 8 Fourier terms the results of the calculation are quite close to those obtained with many more terms. When designing complicated structures it is found to be extremely useful to perform calculations with only a few Fourier terms, until the structural composition is close to what is desired, then repeat the calculations with many more terms to obtain accurate results.

### **III. Self consistency**

Although this model is applicable to any heterostructure formed from bulk III-V or II-VI semiconductors, we have been most concerned with modelling the band structure of the crossed band gap system InAs/GaSb. In this case for wider period structures intrinsic charge transfer takes place from the GaSb to InAs layers [30,31], which leads to significant but slowly varying

contributions to the potential due to Coulomb effects. This requires the introduction of a self-consistent routine, which can also allow us to model the effects of selective doping in heterostructures. To do this we have developed a self-consistent component to solving the band structure so as to account for the single particle Coulomb contribution of the occupied bands. We will first outline the self-consistent procedure, and then discuss how this is manipulated in Type II systems with highly coupled bands.

The band structure is initially calculated using a flat band potential, without considering the effects of the Coulomb potential. This enables us to model any structure without prior knowledge of the band structure or the constituent elements that make up the superlattice. Although an initial guess of the band-edge potential can speed up convergence, we find that the lack of an initial guess costs no more than three iterations in the worst case. The next stage is to evaluate the position of the Fermi level, which is done such that charge neutrality exists throughout the structure, and must account for: occupation of electron states below the Fermi level, occupation of holes above the Fermi level, and the effects of extrinsic doping. Given the position of the Fermi level the carrier occupation of the bands can be evaluated, which enables us to derive the self-consistent potential. This is built up from: the band offsets of the materials, the Coulomb potential of the occupied states and the Coulomb potential of the doping. The Coulomb potentials of the occupied states and doping contributions are derived using Poisson's equation:

$$-\nabla^2 V = \frac{\rho(z)}{\epsilon_r} \quad (11)$$

where  $\rho(z)$  represents the spatial variation of the charge which is derived directly from the summation of the wavefunctions of the occupied states added to the spatial variation of the donors or acceptors. Conventionally in Type I structures the summation over electron and hole like charges is trivial. For example, taking a AlAs/GaAs quantum well, the  $n$ -type charge is

summed over states above the GaAs conduction band, and the  $p$ -type charge is summed over charge below the GaAs valence band. This is not however always true, especially for Type II structures, and this is discussed in detail later. The Coulomb potential is then obtained by integrating the charge distribution twice, with the two constants of integration simply representing the electric field across the superlattice (usually set to zero) and the zero of energy (which is set to the bottom of the conduction band).

The self-consistent potential is then added to the band offsets between the materials, and the band structure re-calculated using this potential. For most of the calculations presented in this paper self-consistency was reached within twelve iterations, though for more complicated structures over twenty iterations were needed. To aid convergence a mixture of the current and previous potentials are used to avoid oscillating solutions.

#### **IV. Defining charge in Type II structures**

In this section of the paper, we present calculations on InAs/GaSb superlattices using the MMM, to examine the nature of electron-hole (e-h) mixing in Type II heterostructures. It is found that the Type II band alignment causes much enhanced e-h mixing, which makes the definition of charge in these structures non-trivial. Furthermore we show how this can be overcome when deriving the Coulomb contribution of the bands, so as to be able to perform self-consistent calculations in such structures.

Before defining the charge we need to understand the nature of electron-hole coupling in Type II structures and how it differs from the Type I case. To compare the two we look at the spinor components of the lowest ‘electron’ subband for the two cases, Type I and Type II. We first present a calculation on an InAs/GaSb superlattice where the band alignment is altered so as to confine the carriers in a Type I arrangement. The only difference between this calculation and

the later modelling performed on a Type II InAs/GaSb structure is the band offsets between the bulk valence bands. Hence we are simply studying the effects of confining the carriers in the two different configurations; it should be noted that we are not varying the intrinsic bulk interband coupling found in the constituent bulk materials that make up the heterostructure. The structure modelled has equal well and barrier widths of 75 Å, and a positive band offset of 150 meV from the GaSb to InAs valence bands (this contrasts with the usual band offset of -560 meV in InAs/GaSb heterostructures). The wavefunctions and band dispersions of the confined states are shown in Fig. 2. A single electron subband and four hole subbands (three heavy hole and one light hole) are confined in the InAs layer. The spinor components of the multi-component envelope functions for the ground electron subband  $E_0$ , are plotted in Fig. 3. The proportion of the electron basis is high, being above 85% for low  $k$ -parallel values, which is very much as expected as the Type I band alignment restricts the interband coupling primarily to the overlap of the electron and hole states in the InAs layer. This is the same type of coupling seen in bulk InAs and described by Kane using 3 band k.p theory. The states in the ground electron subband would be rightly called electrons, and to obtain the charge one integrates over all these states and counts them as contributing to  $n$ -like charge.

The same calculation is now performed on the same structure with the band alignment corrected to represent that of InAs/GaSb (with the InAs conduction band lying 150 meV below the GaSb valence band). The structure is semi-conducting, but with an indirect band gap, the electron states lying *mainly* in the InAs layer and the hole states *mainly* in the GaSb layer; fig. 4 shows the wavefunctions and band dispersions for the confined states. The proportion of the spinor bases for the ground electron subband is displayed in Fig. 5. The electron-hole coupling is much enhanced in the Type II variant compared with its Type I counterpart, the electron basis

being restricted to between 60 % and 75 %. The mixing is dominated by the light holes at low  $k$ -parallel values but there is even a large heavy hole component at higher  $k$ -values (the dependence on superlattice wavevector  $q$  has been described before [32]). This enhanced e-h coupling within the electron subband is due to two main factors; firstly the energy difference between  $E_0$  and the bulk valence band of GaSb is small thus enhancing coupling; and secondly due to interband coupling in the InAs layer the light hole component of the  $E_0$  subband has a maximum at the InAs/GaSb interface, and thus propagates strongly into the GaSb layer. Analysis of the envelope functions of the light hole spinor component shows that they have strong components in both layers, and most importantly the component within the InAs layer is stronger than in the Type I case, due to this propagation. Thus the strong e-h coupling is a consequence of both Kane like bulk interband e-h coupling as seen in the Type I structure, and also to the extended propagation of the light hole component envelope function in both layers.

This has important consequences when considering the definition of charge in the structure. For the purposes of the following discussion we split the integration of the charge up into four distinct contributions:

1. 's' like components within the InAs layer
2. 'p' like components within the InAs layer
3. 's' like components within the GaSb layer
4. 'p' like components within the GaSb layer

where 's' and 'p' refer to electron and hole like atomic bases. If we use the 'bulk approximation' we would integrate the  $n$ -type charge as the sum of the first and second contributions for all states defined as electrons, and similarly for  $p$ -type charge a sum is performed over the third and fourth contributions for all states defined as holes (the definition of electron like or hole like

coming from a simple majority analysis of the component atomic bases). This has obvious advantages as the charge is calculated in the same manner as is performed for bulk materials, but this neglects two facts; firstly we are neglecting to account for the ‘s’ like components in the GaSb layer, which are due to the natural propagation of the envelope functions of the electron subbands into the barrier layer; secondly, it has been shown above that the ‘p’ like states in the InAs layer are stronger in a Type II system (compared to Type I structures) due to interlayer light hole coupling to electron states, which would increase the calculated charge density (as well as distorting the spatial distribution of the charge in the well).

To address these problems we have redefined the way in which we look at charge, by considering the ‘s’ and ‘p’ like nature of the states as opposed to the usual electron/hole definition. What we are able to avoid is the arbitrary definition of a state with only 55% ‘s’ like atomic bases as being an ‘electron’, and instead say that this state is 55% electron like and 45% hole like (this is directly analogous to describing the state using fuzzy set theory instead of classical set theory [ref.33]). In the following discussion we consider two heavily mixed states one below the Fermi level and one above the Fermi level. For the former case (below the Fermi level) we consider the sum over the ‘s’ like wavefunctions and consider this as electron like charge that is added to the potential; in the latter case the summation is performed over the ‘p’ like states and this adds hole like charge to the superlattice potential. Writing this explicitly, the electron ( $n$ ) and hole ( $p$ ) like charge is given by:

$$n = \int_{-\infty}^{E_F} \sum_n |f_n |u_n(s)\rangle|^2 dE \quad p = \int_{E_F}^{\infty} \sum_n |f_n |u_n(p)\rangle|^2 dE \quad (12)$$

where  $u_n(s)$  and  $u_n(p)$  represent the ‘s’ and ‘p’ like atomic Kane bases as given in Table 1. The summations are taken over all subbands, with the dependence of the envelope function on  $k$ -parallel included to take account of the mixing away from the zone centre. Using this method a

particular state only contributes electron or hole charge and not both at the same time. The inclusion of the s-like contribution of valence band states in the sum for the electron density makes up for the mixing of the valence band into the conduction band. The total charge transfer from one layer to the other can then be evaluated by looking at the total charge distribution in the structure. One problem with this method, however, is that it requires the treatment of a complete set of all mixed states which it is difficult to achieve practically. In particular the strong electron-light hole coupling found in the electron subbands leads to a larger contribution from hole like states than electron like states in the region above the InAs conduction band. As a result in a real calculation we find that the Fermi energy is too high in energy often lying above the highest confined heavy hole subband (the hole charge being built up from the strong light hole components in the electron subbands which lie above the GaSb valence band edge). To deal with this would require a sum over an impracticably large number of balancing hole states. To rectify this simply we put a constraint on the energy window over which the Fermi energy is calculated, such that we integrate the charge between the lowest confined electron level  $E_0$  and highest confined hole level  $H_0$ . Thus Equ. 12 is modified as shown below:

$$n = \int_{E_0}^{E_F} \sum_n |f_n |u_n(s)\rangle|^2 dE \quad p = \int_{E_F}^{H_0} \sum_n |f_n |u_n(p)\rangle|^2 dE \quad (13)$$

where  $E_0$  is defined as the lowest energy state with a total 's' basis greater than 0.45, and  $H_0$  is defined as the highest energy state with a total 'p' basis greater 0.5. The choice of 0.45 for definition of the lowest lying electron state (instead of 0.5) is arbitrary, but it is found that this results in a more realistic Fermi energy position. Although we have had to return to describing a state as being an 'electron' or 'hole', this is used solely for determining the calculation window, and not to obtain the state's contribution to the charge density. Using this method we have been

able to successfully model the charge in the strongly coupled InAs/GaSb system as shown by the series of examples given in the following section.

## V. Applications

### 1. Semimetallic InAs/GaSb superlattices

In this section we concentrate on calculations performed on InAs/GaSb semimetallic superlattices. The system is well known for the unusual crossed band alignment with the InAs conduction band lying approximately 150 meV above the GaSb valence band edge [30,31]. In early modelling of this system the calculations were performed non-self-consistently with the band offset between the two materials artificially altered so as to fit the data. In recent years experimental data has confirmed that the offset is  $\sim 150$  meV [34], and so it seems best to perform self-consistent calculations without adjusting the offset. The materials parameters used in these calculations are quoted in Appendix A.

So as to compare the results from the momentum matrix technique with those performed using the transfer-matrix technique, we have chosen to mimic the InAs/GaSb superlattice that was presented by Altarelli [35] with an InAs layer width of  $120 \text{ \AA}$  and a GaSb layer width of  $80 \text{ \AA}$ . The calculation is performed self-consistently with convergence being reached in 7 iterations, and the number of Fourier terms used was 12. The dispersion along  $k_x$  and the superlattice direction  $k_z$  is plotted in Fig. 6. Although we are using slightly different band parameters, different Hamiltonians and different techniques, we obtain similar results. We observe a small direct energy gap of 3.9 meV at  $k_z=\pi/d$ ,  $k_{||}=0.057$  which compares with Altarelli's findings of a gap with energy 2 meV at  $k_z=\pi/d$ ,  $k_{||}=0.043$ . The valence band dispersions are slightly different

for lower-lying bands, but this is probably due to Altarelli's use of the spherical approximation, and different Luttinger parameters. The influence of the number of Fourier terms used is shown in Table 2, which shows how the band edge solutions vary, together with the carrier density. Reasonable consistency is reached by the use of 12-16 terms in this case, giving an accuracy of order 0.1 meV.

Recent interest in this material system has concentrated on the anticrossing between the ground electron ( $E_0$ ) and ground hole ( $HH_0$ ) levels which we term the minigap [36-40]. The calculation shows that this varies strongly with the superlattice wavevector  $q$  from 3.9 meV at ( $q=\pi/d, k_{\parallel}=0.057$ ) to 22.9 meV at ( $q=0, k_{\parallel}=0.067$ ). The large change in minigap energy with the superlattice wavevector is explained by symmetry constraints on interband mixing in Type II systems [32].

## **2. InAs/GaSb single heterojunctions**

The study of InAs/GaSb single heterojunctions is of interest due to the unusual band alignment which causes negative differential resistance (NDR) [41]. Using the model shown above we can calculate the band structure of a single heterojunction at finite electric field to show the effects on the electron and hole levels as they cross and become decoupled. Such calculations are performed on wide layered structures with single layers of InAs and GaSb both of which have a width 500 Å. An external electric field is placed across the structure so as to investigate the electron and hole states at the point when NDR occurs. Although the boundary conditions used in the calculation are those for a superlattice the wide layers result in virtually no overlap of the states in neighbouring wells and hence the calculation mimics a single heterojunction. The calculation is performed self-consistently, although it should be noted that

calculations which include both the effects of electric field and self-consistency cannot be extended for more complex structures (as seen later with the quantum cascade structures) as problems arise in the determination of a realistic Fermi level.

An example of the results for such a calculation are shown in Fig. 7, for a structure with an electric field of  $4\text{MVm}^{-1}$  across the  $1000\text{ \AA}$  structure. The calculation was performed with 15 Fourier terms, and takes into account the charge transfer across the interface using the self-consistent routine outlined above. The band bending at the InAs/GaSb interface is seen to resemble that expected for a single heterojunction [42]. In the following we concentrate on the confinement of the states at either side of the heterojunction interface, the states being confined by a combination of the electric potential across the bulk materials and the self-consistent Coulomb potential of the occupied states. For the structure shown in Fig. 7 a negative band gap of  $30.9\text{ meV}$  exists at  $k_{\parallel}=0$  with the resulting charge transfer between the two layers resulting in  $n$  and  $p$  charge densities of  $2.6\times 10^{11}\text{ cm}^{-2}$ . As in the superlattice calculation outlined above a small anticrossing occurs close to the Fermi level between the ground electron and hole states. The minigap energy however is much smaller ( $1.7\text{ meV}$  compared with  $22.9\text{ meV}$  for the superlattice structure) and shows how the interlayer coupling strongly decreases with only a single interface present.

To observe the effects of electric field on the confinement of the states, we have performed a series of calculations at a number of different electric field values. The results are shown in Fig. 8. At the lowest electric field value of  $1.5\text{ MVm}^{-1}$  the structure is shown to have a negative band gap of  $49\text{ meV}$ , the gap decreasing strongly with increasing electric field. At electric fields above  $8\text{MV/m}$  the bands are decoupled and a small band gap semiconductor exists.

In this case charge transfer no longer takes place and the calculation can only be performed non-self-consistently.

### 3. Semimetallic InAs/GaSb heterostructures at finite magnetic field

There has been much recent interest both experimentally and theoretically in the cyclotron resonance of a single InAs layer clad with regions of GaSb barrier material [43-46]. The amplitude and linewidth of the cyclotron resonance is seen to oscillate with field and has been recently attributed to the minigap-like anticrossing between electron and hole states [45,46]. Modelling of InAs/GaSb structures at finite magnetic field is thus of current interest to understand this phenomena. In this paper we present two sets of calculations firstly on InAs/GaSb superlattices, and secondly extending the modelling performed on InAs/GaSb heterojunctions seen in the previous section to finite electric and magnetic field.

Fig. 9 shows the energies of the Landau levels for a superlattice consisting of 200Å InAs and 50Å GaSb layers at  $q=0$  and  $q=\pi/d$ . The calculation has been performed with the assumption that the system has a very small net  $n$ -type doping ( $1 \times 10^7 \text{ cm}^{-2}$ ), with the result that at the highest fields the Fermi level follows the lowest electron Landau level. The results show that there is a large and clearly visible minigap coupling for the  $q=0$  states, the coupling occurring between electron and hole levels with the same total angular momentum quantum number ( $n$ ), but for the  $q=\pi/d$  states the coupling is substantially reduced. In both cases ( $q=0$  and  $q=\pi/d$ ) as the levels of the electrons and holes cross each other there are non-linear increases in the energy levels with magnetic field due to the changes to the self-consistent potential caused by the change in the number of occupied levels. The graphs also show the position of the Fermi level and the electron carrier density which show more clearly the oscillatory nature of the energies.

For magnetic fields above 30 T there is a steady reduction in carrier density as the last few levels begin to uncross, and by 50 T the carrier density has fallen to essentially zero. In the region 30 - 50 T the levels vary relatively slowly with field as the change in the self-consistent potential acts to balance the change in density.

Figure 10 shows the results of a calculation for a single heterojunction of InAs with GaSb subject to an electric field of  $5 \text{ MVm}^{-1}$  (which is modelled as a superlattice with a large potential offset between thick adjacent layers as in the previous section). In this case there is no superlattice coupling along the growth direction and therefore no dispersion for the momentum along the growth direction. As a result the density of states is much more singular and therefore the oscillatory nature of both the energy levels and the carrier density has become much more pronounced. As there is only one interface in this structure the magnitude of the anticrossing features is however much reduced.

#### **4. Quantum cascade structures**

There has been much recent interest in the design and fabrication of quantum cascade devices, emitting infrared radiation in the region  $5 - 12 \mu\text{m}$ . Quantum cascade structures contain a staircase of quantum wells where the injected electrons are recycled, enabling the quantum efficiency (the number of photons emitted per electron) to exceed 100% [47-48]. In this paper we have used the momentum matrix technique to model InAs/GaSb quantum cascade structures, with the emphasis on using the unusual band alignment of the system to reduce the complexity of the structures. We present the idea of minigap assisted tunnelling in InAs/GaSb quantum cascade structures, and propose cascade devices without injector and collector regions.

Careful control of the band structure means that the carriers from one active layer tunnel straight into the next active region by means of the strong coupling between electrons and holes.

The proposed structure is essentially an InAs/GaSb superlattice with the layer widths and electric field across the device carefully controlled so as to introduce strong electron-hole coupling between the energy levels in adjacent materials. Fig. 11 shows the energy levels for such a superlattice with electric field along the growth direction, calculated using **k.p** modelling. The calculation is different from the modelling performed in the previous examples. The ‘superlattice unit cell’, which the superlattice Bloch condition operates over, contains 5 periods each containing an InAs and GaSb layer. This is necessary to observe cascade effects over a number of periods. The inclusion of electric field is simple and is a linear function added onto the potential profile of the bands. The momentum matrix technique is easily able to accommodate this variation of potential and in essence no changes are made to the model used. The calculation is not performed self-consistently as carriers would accumulate at the minimum of the potential profile.

The wavefunctions are plotted in Fig. 11, for a superlattice with an InAs well width of 160 Å and GaSb barrier width of 80 Å. An electric field of 120 meV is placed across each superlattice period (one layer of InAs and GaSb). The active transition is intersubband in nature between the  $E_1$  and  $E_0$  subbands in the InAs wells (denoted by an arrow). The key to the structure is aligning the  $E_0$  subband in well A with the ground hole subband in the barrier (B). This is intended to ensure that the electrons from  $E_0$  can escape from the well quickly. The structure is also designed such that the ground hole subband in the barrier (B) is aligned with the subband  $E_1$  in well C, which forms the initial state of the next active region. The structure relies on strong interlayer coupling between the states in the different layers, so as to transfer the

electrons from one active region to the next. From the initial calculation it can be seen that strong wavefunction overlap does exist between the final state ( $E_0$ ) in well A and the initial state ( $E_1$ ) in well C. This coupling is enhanced further by the coupling of the electron levels to the heavy hole subband in the barrier material. The electron-hole coupling is strongly enhanced by the in-plane momentum which can be seen in Fig. 11b where the HH level is seen to anticross strongly with both of the electron levels over a range of only 10meV.

#### **IV. Conclusions**

In this paper we have demonstrated the use of the ‘momentum matrix technique’ which is an extremely flexible approach to calculating the band structure of heterostructures. Based on the standard envelope function approach of the  $k.p$  formalism, the method builds on earlier work [21] to solve the band structure of semiconductor heterostructures in  $k$ -space thus avoiding the problems associated with spurious solutions found in transfer matrix techniques. We have described a self-consistent routine which is able to account for strong electron-hole coupling between the states and thus enables us to model broken gap heterostructures such as InAs/GaSb. This technique easily enables a wide variety of properties to be modelled including: band bending, doping, electric fields, interface charges, strain, graded composition and interlayer coupling.

## References

- [1] J. W. Luttinger, *Phys. Rev.* **102** 1030 (1956)
- [2] C. R. Pidgeon and R. N. Brown, *Phys. Rev.* **146** 575 (1966)
- [3] E. O. Kane, in: *Handbook on Semiconductors*, Ed. T. S. Moss, (North-Holland. 1982) pg. 193
- [4] M. H. Weiler, in *Semiconductors and Semimetals*, Vol. 16, edited by R. K. Willardson and A. C. Beer, Academic Press, 1981, page 119.
- [5] W. Zawadzki, S. Klahn, U. Merkt, *Phys. Rev. B* 33 6916 (1986)
- [6] M. Altarelli and G. Platero, *Superlat. and Microst.* 5 499 (1989)
- [7] J. Faist, F. Capasso, C. Sirtori, D. L. Sivco, A. L. Hutchinson, M. S. Hybertsen, A. Y. Cho, *Phys. Rev. Letts.* 76 411 (1996)
- [8] D.L Smith and C. Mailhot, *Rev. Mod. Phys.* **62** 173 (1990)
- [9] S. S. Nedorezov, *Sov. Phys.-Solid State* 12 1814 (1971)
- [10] M. G. Burt, *Semicond. Sci. Technol.* 3 739 (1988)
- [11] L. R. Ram-Mohan, K. H. Yoo, R. L. Aggarwal, *Phys. Rev. B* 38 6151 (1988)
- [12] G. Bastard, *Phys. Rev. B* 24 5693 (1981)
- [13] G. Bastard, *Phys. Rev. B* 25 7584 (1982)
- [14] K. I. Kolokolov, A. M. Savin, S. D. Beneslavski, N. Ya. Minina, *Phys. Rev. B* 59 7537 (1999)
- [15] A. Baliga, D. Trivedi, N. G. Anderson, *Phys. Rev. B* 49 10402 (1994)
- [16] J. P. Cuypers and W. van Haeringen, *Phys. Rev. B* 47 10310 (1993)
- [17] S. de-Leon, B. Laikhtman, L. D. Shvartsman, *J. Phys. Cond. Mat.* 10 8715 (1998)
- [18] B. A. Foreman, *Phys. Rev. Lett.* 81, 425 (1998)

- [19] S. R. White and L. J. Sham, Phys. Rev. Lett. 47 879 (1981)
- [20] L.W. Wang and A. Zunger, Phys. Rev. B 59 15806 (1999)
- [21] R. Winkler and U. Rossler, Phys. Rev. B 48 8918 (1993)
- [22] G. Bastard, in Proceedings of the NATO advanced study institute on molecular beam epitaxy in heterostructures, Erice, Italy, 1993, edited by L. L. Chang and K. Ploog (Martinus-Nijhoff, Dordrecht, 1984) pg. 381
- [23] D. L. Smith and C. Mailhot, Phys. Rev. B 33 8345 (1986)
- [24] Y-C. Chang, Phys. Rev. B 37 8215 (1988)
- [25] G. A. Sai-Halasz, L. Esaki, W. A. Harrison, Phys. Rev. B 18 2812 (1978)
- [26] M. L. Cohen and T. K. Bergstresser, Phys. Rev. 141 789 (1966)
- [27] R. A. Morrow and K. R. Brownstein, Phys. Rev. B 30 678 (1984)
- [28] A. M. Cohen and G. E. Marques, Phys. Rev. B 41 10608 (1990)
- [29] G. Y. Wu, T. C. McGill, C. Mailhot, D. L. Smith, Phys. Rev. B 39 6060 (1989)
- [30] L. L. Chang, Heterojunctions and Superlattices, Eds. G. Allan, G. Bastard, N. Bocaara, M. Lanno, M. Voos (Springer, Berlin 1986) pg. 152
- [31] Y. Guldner, J. P. Vieren, P. Voisin, M. Voos, J. C. Maan, L. L. Chang, L. Esaki, Solid State Commun. 41 755 (1982)
- [32] P. Voisin, G. Bastard, M. Voos, Phys. Rev. B 29 935 (1984)
- [33] L.A. Zadeh, Journal of Information and Control 8 338 (1965)
- [34] D. M. Symons, M. Lakrimi, R. J. Warburton, R. J. Nicholas, N. J. Mason, P. J. Walker, M. I. Eremets, G. Hill, Phys. Rev. B 49 16614 (1994)
- [35] M. Altarelli, Phys. Rev. B 28 842 (1983)
- [36] M. Lakrimi, S. Khym, R. J. Nicholas, D. M. Symons, F. M. Peeters, N. J. Mason, P. J. Walker, Phys. Rev. Lett. **79** 3034 (1997)

- [37] M. J. Yang, C. H. Yang, B. R. Bennet, B. V. Shanabrook, Phys. Rev. Lett. 78 4613 (1997)
- [38] A. J. L. Poulter, M. Lakrimi, R. J. Nicholas, N. J. Mason, P. J. Walker, Phys. Rev. B 60 1884 (1999)
- [39] J-C. Chiang, S-F. Tsay, Z. M. Chau, I. Lo, Phys. Rev. Lett. 77 2053 (1996)
- [40] Y.Naveh and B. Laikhtman, Appl. Phys. Lett. 66 1980 (1995)
- [41] U. M. Khan-Cheema, N. J. Mason, P. J. Walker, P. C. Klipstein, G. Hill, J. Phys. Chem. Solids 56 463 (1995)
- [42] U. M. Khan-Cheema, D. Phil thesis, University of Oxford 1996 (unpublished)
- [43] J. Kono, B. D. McCombe, J.-P. Cheng, I. Lo, W. C. Mitchel, C. E. Stutz, Phys. Rev. B 57 12242 (1994)
- [44] R. J. Warburton, B. Brar, C. Gauer, A. Wixworth, J. P. Kotthaus, H. Kroemer, Solid State Elect. 40 679 (1996)
- [45] S. D. Suchalkin, Y. B. Vasilyev, K. VonKlitzing, V. N. Golovach, G. G. Zegrya, S. V. Ivanov, P. S. Kopev, B. Y. Meltser, JETP Lett. 68 792 (1998)
- [46] T. P. Marlow, L. J. Cooper, D. D. Arnone, N. K. Patel, D. M. Whittaker, E. H. Linfield, D. A. Ritchie, M. Pepper, Phys. Rev. Lett. 82 2362 (1999)
- [47] F. Cappasso, J. Faist, D. L. Sivco, C. Sirtori, A. L. Hutchinson, A. Y. Cho, Science 264 553 (1994)
- [48] R. Q. Yang and S. S. Pei, J. Appl. Phys. 79 8197 (1996)

## TABLES

**Table 1:** The Kane basis states used to describe the bulk band structure. The column labelled ‘State’ indicates the nature of the basis function when calculating the charge density in strongly mixed bands.

$ J, m_J\rangle$ $n$	BASIS FUNCTION $u_n(\mathbf{r})$	STATE $s$ or $p$	ENERGY $E_n^\Gamma$	BAND
$ \frac{1}{2}, \frac{1}{2}\rangle$	$ S \uparrow\rangle$	$u_0(s)$	0	Conduction
$ \frac{3}{2}, \frac{3}{2}\rangle$	$\frac{-i}{\sqrt{2}}( X \uparrow\rangle + i Y \uparrow\rangle)$	$u_1(p)$	$-E_g$	Heavy Hole
$ \frac{3}{2}, -\frac{1}{2}\rangle$	$\frac{i}{\sqrt{6}}( X \uparrow\rangle - i Y \uparrow\rangle + 2 Z \downarrow\rangle)$	$u_2(p)$	$-E_g$	Light Hole
$ \frac{1}{2}, -\frac{1}{2}\rangle$	$\frac{-i}{\sqrt{3}}( X \uparrow\rangle - i Y \uparrow\rangle -  Z \downarrow\rangle)$	$u_3(p)$	$-E_g - \Delta$	Spin-Orbit
$ \frac{1}{2}, -\frac{1}{2}\rangle$	$ S \downarrow\rangle$	$u_4(s)$	0	Conduction
$ \frac{3}{2}, -\frac{3}{2}\rangle$	$\frac{i}{\sqrt{2}}( X \downarrow\rangle - i Y \downarrow\rangle)$	$u_5(p)$	$-E_g$	Heavy Hole
$ \frac{3}{2}, \frac{1}{2}\rangle$	$\frac{-i}{\sqrt{6}}( X \downarrow\rangle + i Y \downarrow\rangle - 2 Z \uparrow\rangle)$	$u_6(p)$	$-E_g$	Light Hole
$ \frac{1}{2}, \frac{1}{2}\rangle$	$\frac{-i}{\sqrt{3}}( X \downarrow\rangle + i Y \downarrow\rangle +  Z \uparrow\rangle)$	$u_7(p)$	$-E_g - \Delta$	Spin-Orbit

**Table 2.** The  $k=0$  solutions for a 120/80 Å InAs/GaSb superlattice calculated using different numbers of Fourier Terms.

Fourier terms	$E_0$	$HH_0$	$E_F$	Carrier density
8	97.45	131.07	125.94	2.69
12	97.56	131.02	125.92	2.67
16	97.57	130.86	125.84	2.66
20	97.57	130.88	125.85	2.66

## APPENDIX A

Material parameters used in the calculations for this work are given in the table below:

Parameter	InAs	GaSb
$E_g$	418	810
Delta	380	775
Gamma1	2.06	4.26
Gamma2	-0.36	0.18
Gamma3	0.4	1.48
F	-0.028	-0.024
Kappa	-1.17	-1.43
Kane	22.2	24.4
a	6.0584	6.0954
$m_e$	0.023	0.042
$m_{hh}$	0.41	0.28
$m_{lh}$	0.025	0.045

## FIGURE CAPTIONS

**Figure 1:** A schematic diagram showing a simple A-B-A-B superlattice. The distances  $d_1$ ,  $d_2$  and  $d$  referred to in the text are shown.

**Figure 2:** The results of a k.p calculation performed on a “Type I” InAs/GaSb structure with equal well and barrier widths of 75 Å. The plot on the left shows the spatial variation of the potentials and confined wavefunctions, the right hand plot showing the dispersion along  $k$ -parallel. The wavefunctions shown are a sum of the squares of the spinor components.

**Figure3:** The proportion of the electron, heavy hole, light hole and spin orbit basis states in the ground electron subband for a “Type I” InAs/GaSb.

**Figure 4:** The results of a k.p calculation performed on a conventional Type II InAs/GaSb structure with equal well and barrier widths of 75 Å. The plot on the left shows the spatial variation of the potentials and confined wavefunctions, the right hand plot showing the dispersion along  $k$ -parallel.

**Figure5:** The proportion of the electron, heavy hole, light hole and spin orbit basis states in the ground electron subband for a conventional Type II InAs/GaSb structure.

**Figure 6:** The dispersion relation in  $k$ -space of the band structure of a semimetallic InAs/GaSb superlattice, mimicking the results seen by Altarelli. The notation in brackets refers to the points in  $k$ -space  $(k_x, k_y, q)$ .

**Figure 7:** The band edge potential and wavefunctions of the confined states of a InAs/GaSb heterojunction calculated using the momentum matrix technique. The electric field across the structure is  $4\text{MVm}^{-1}$ . a). The plot shows the wavefunctions of the confined electron and hole states in the InAs and GaSb layers respectively. The wavefunctions shown are a sum of the squares of the spinor components. The dashed lines represent the conduction and valence bands of the bulk materials and the dotted line is the intrinsic Fermi energy of the structure. b). The dispersion of the heterojunction states in  $k$ -space.

**Figure 8:** The results of a series of calculations performed on InAs/GaSb heterojunctions at differing electric fields. a). The zone centre energies of the electron (squares), heavy hole (circles) and light hole (triangles) confined states of the heterojunction at differing electric fields. Below electric field values of  $9\text{MVm}^{-1}$  the calculations are performed self-consistently, above this value the structure resembles a small band gap semiconductor and no charge transfer takes place. b). The self-consistent carrier density as a function of electric field. The gradient of the plot is shown to change as  $E_1$  ( $3\text{MVm}^{-1}$ ) and  $E_0$  ( $8\text{MVm}^{-1}$ ) become confined above the highest heavy hole level.

**Figure 9:** The energy levels of an InAs/GaSb superlattice ( $200\text{\AA}/50\text{\AA}$ ) are shown at finite magnetic field orientated parallel to the growth direction. The electron levels are shown as

crosses and the hole levels as squares with the carrier density indicated by the dashed line. a): the states at  $q=0$ . b): the states at  $q=\pi/d$ .

**Figure 10:** The energy levels of an InAs/GaSb heterojunction at finite electric and magnetic field.

**Figure 11:** An example of the use of the momentum matrix technique to model quantum cascade structures. a). The wavefunctions of the confined electron and hole states are plotted at ( $k_{//}=0$ ,  $q=0$ ). The wavefunctions shown are a sum of the squares of the spinor components. The dotted lines show the spatial variation of the InAs and GaSb conduction and valence bands, and the arrows mark the radiative intersubband transition. b). The dispersion of the states along  $k_{//}$ , showing the extent of the interlayer coupling.

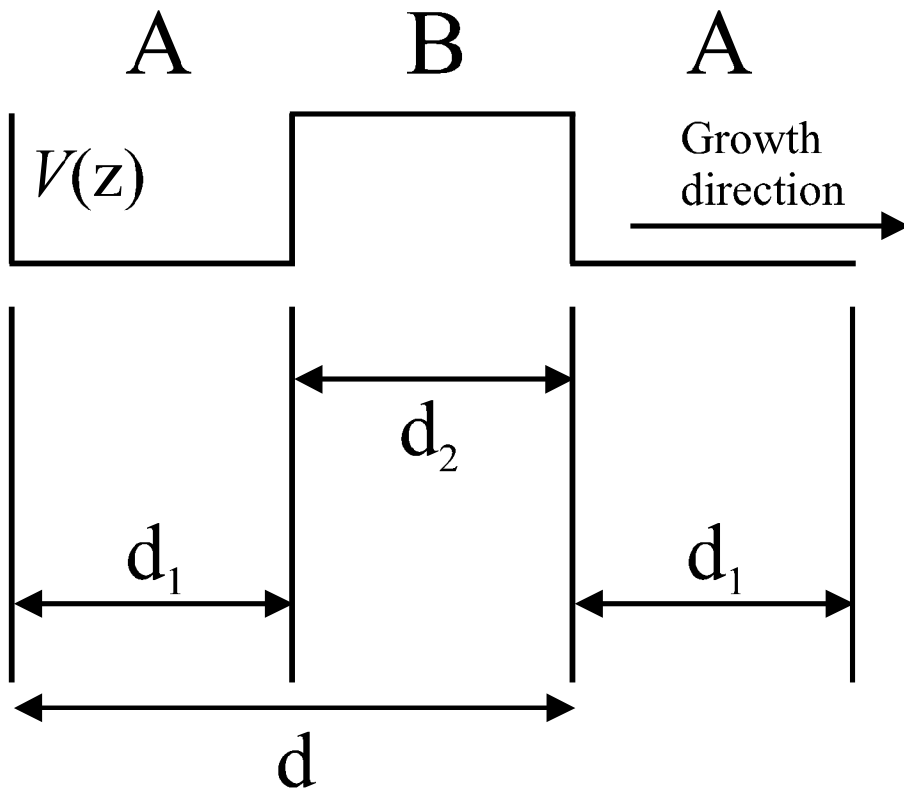


**Fig. 1**

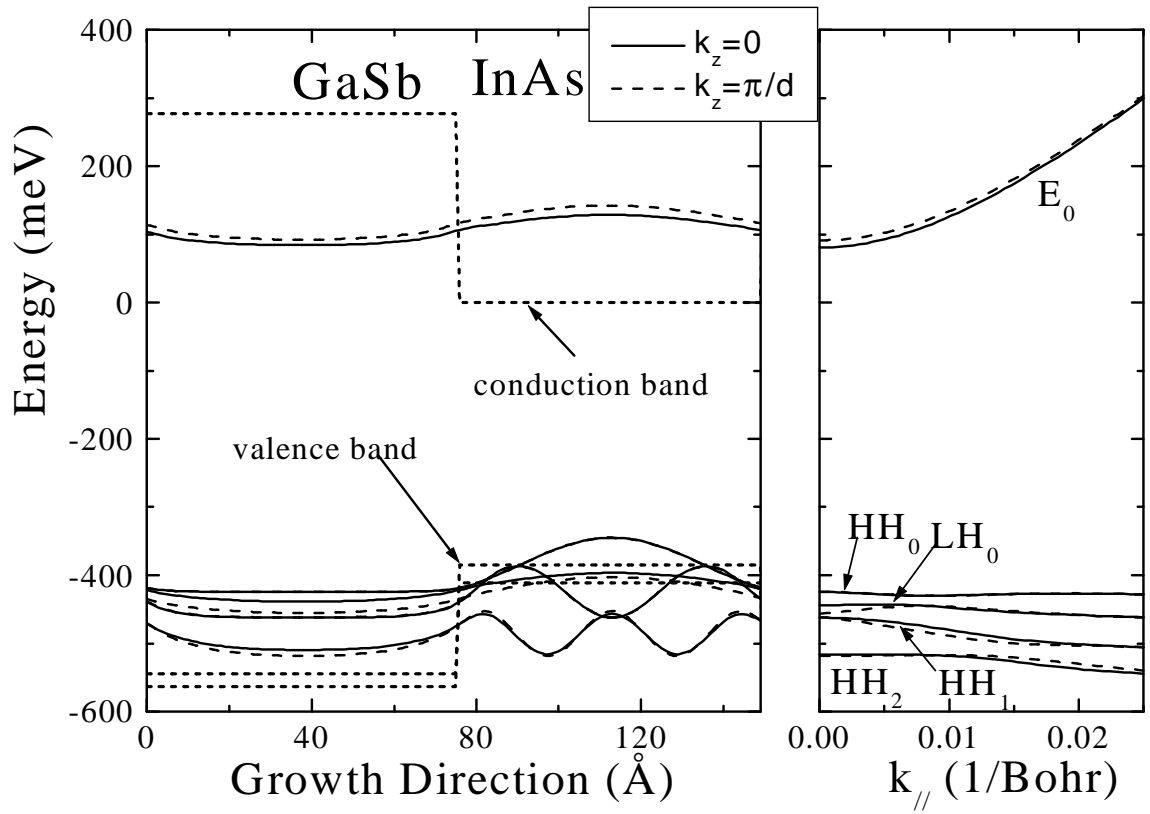
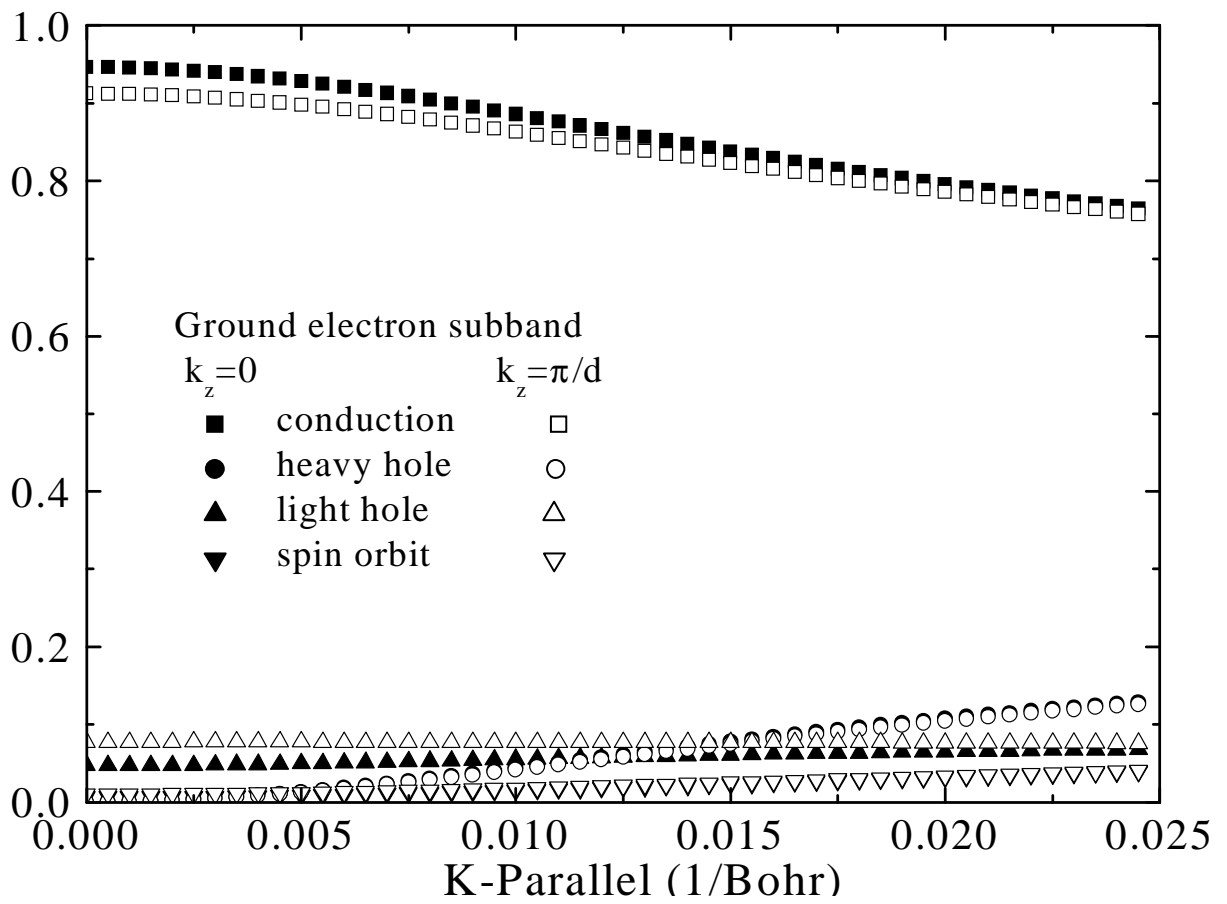
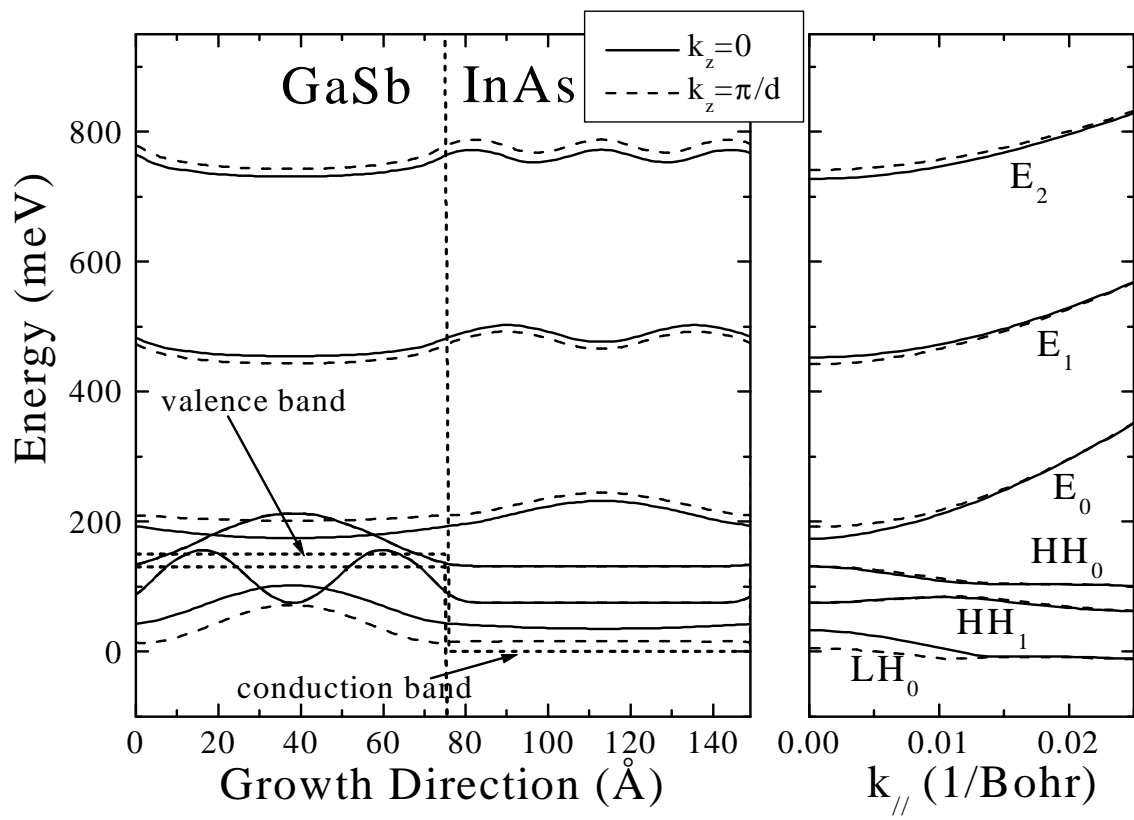


Fig. 2



**Fig. 3**



**Fig. 4**

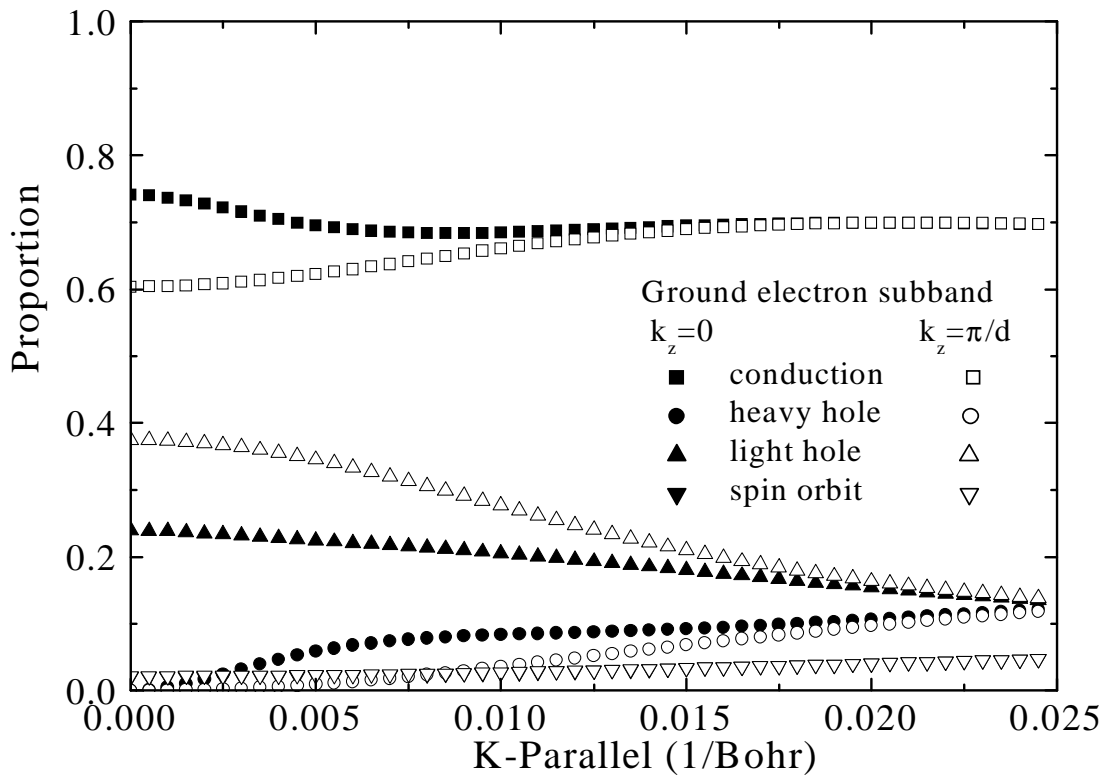
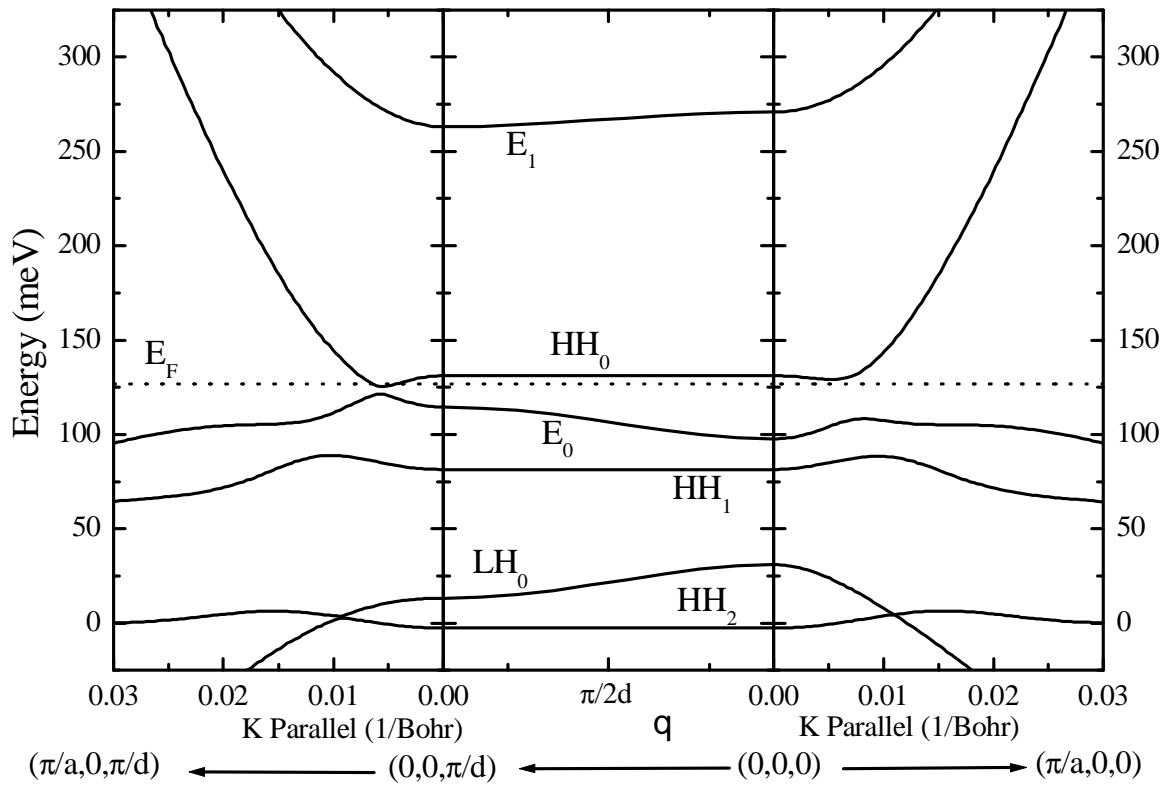
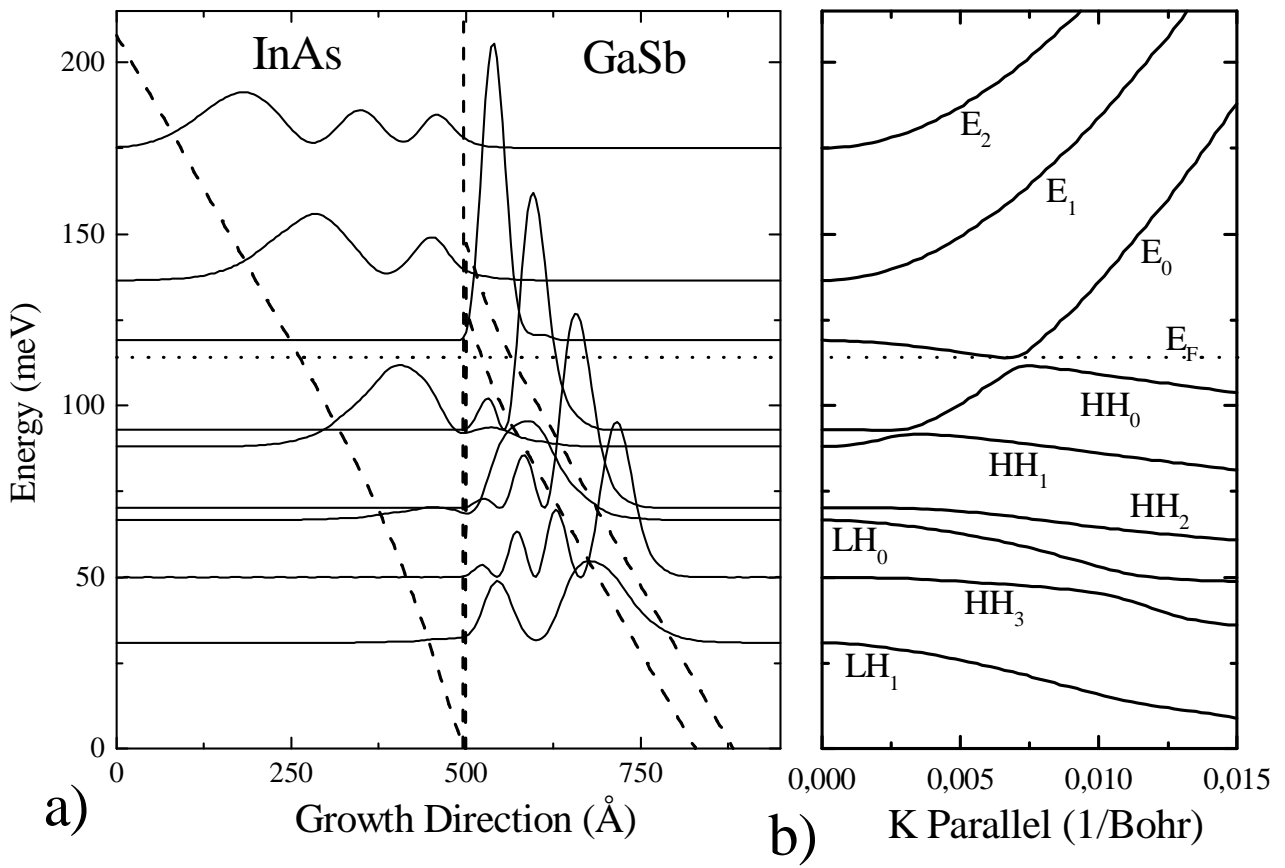


Fig. 5



**Fig. 6**



**Fig. 7**

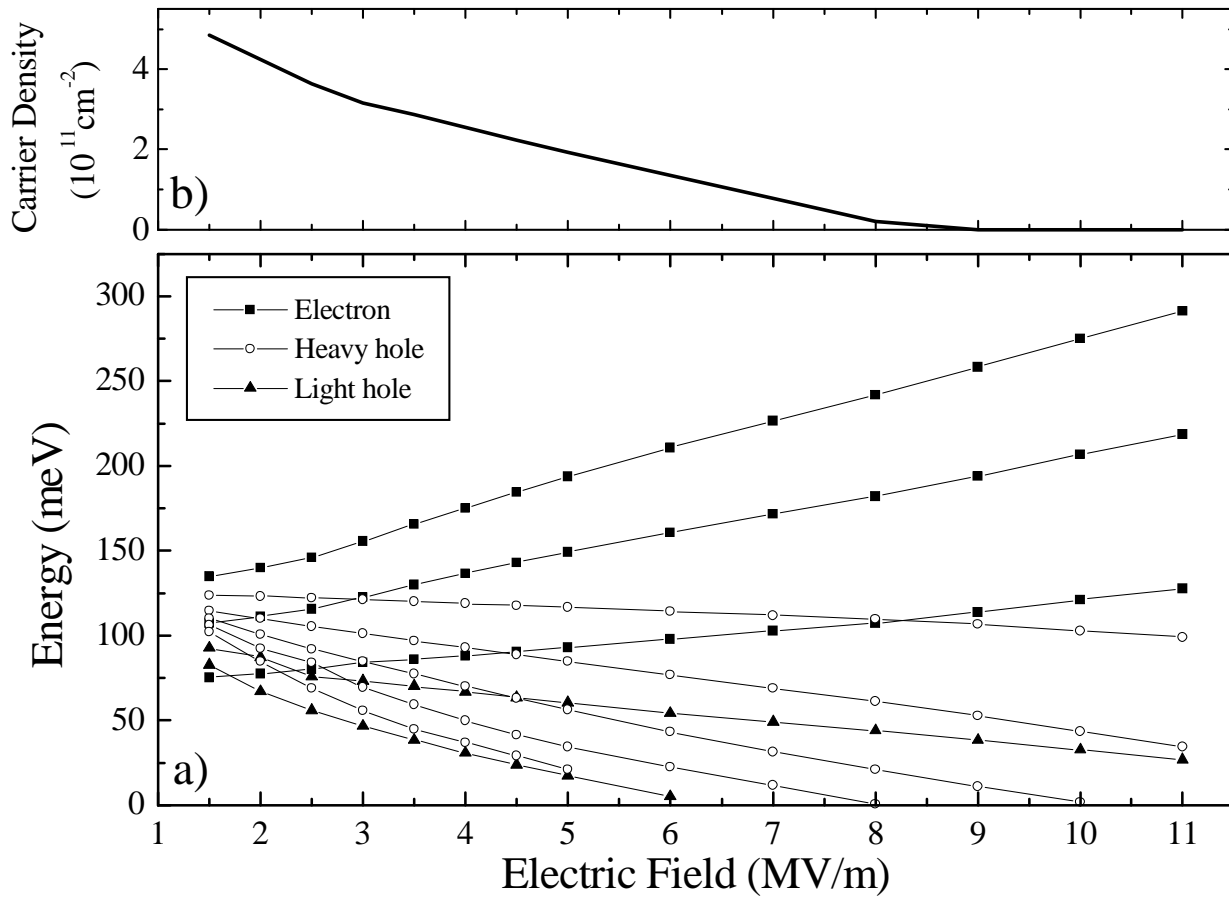


**Fig. 8**

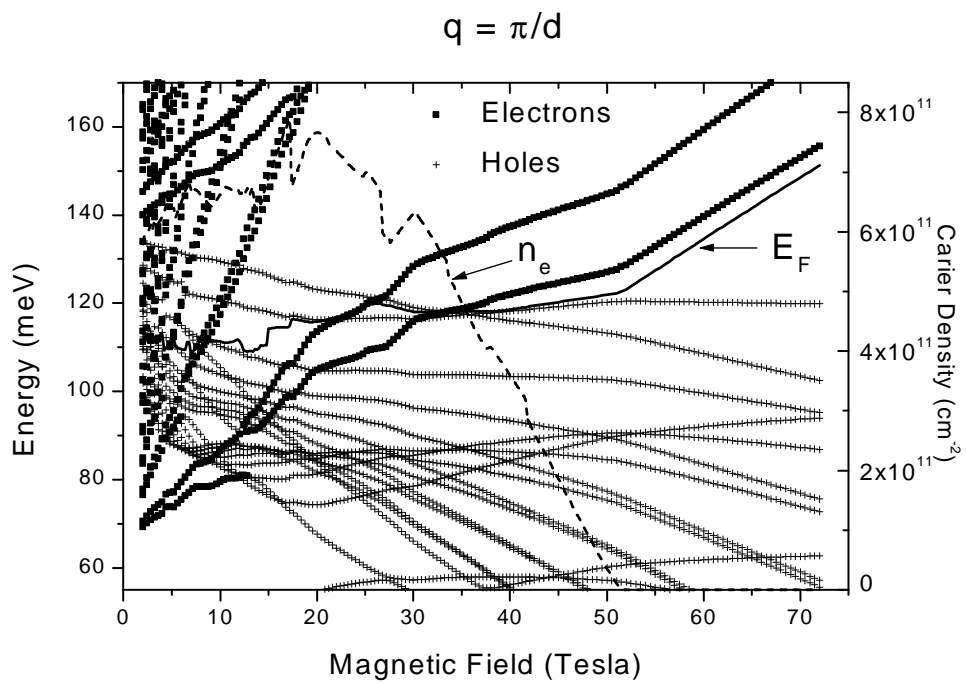
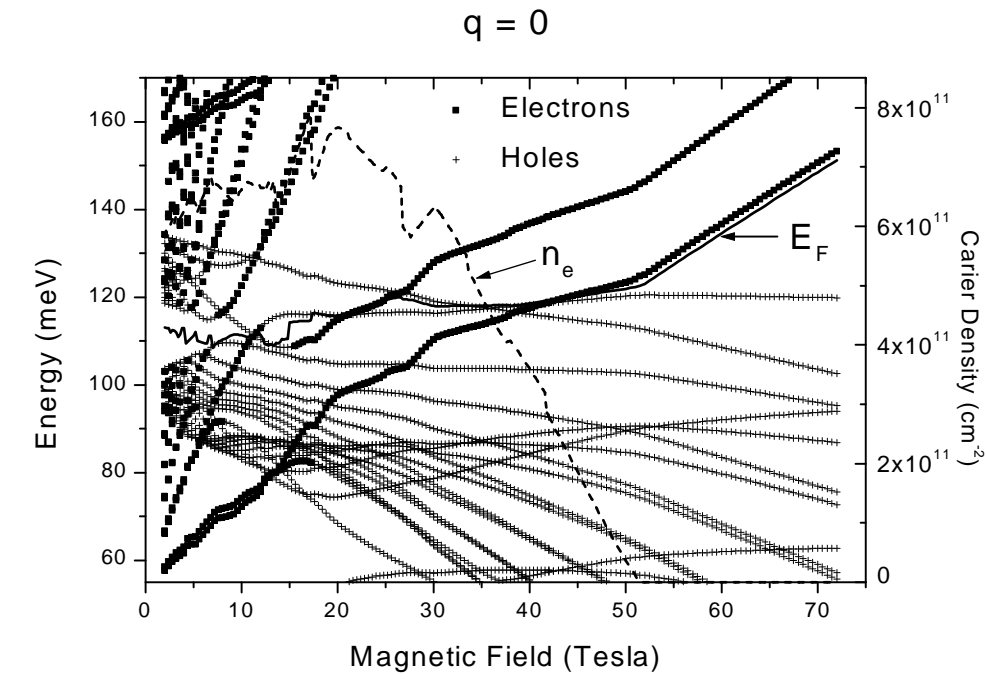


**Fig. 9.**

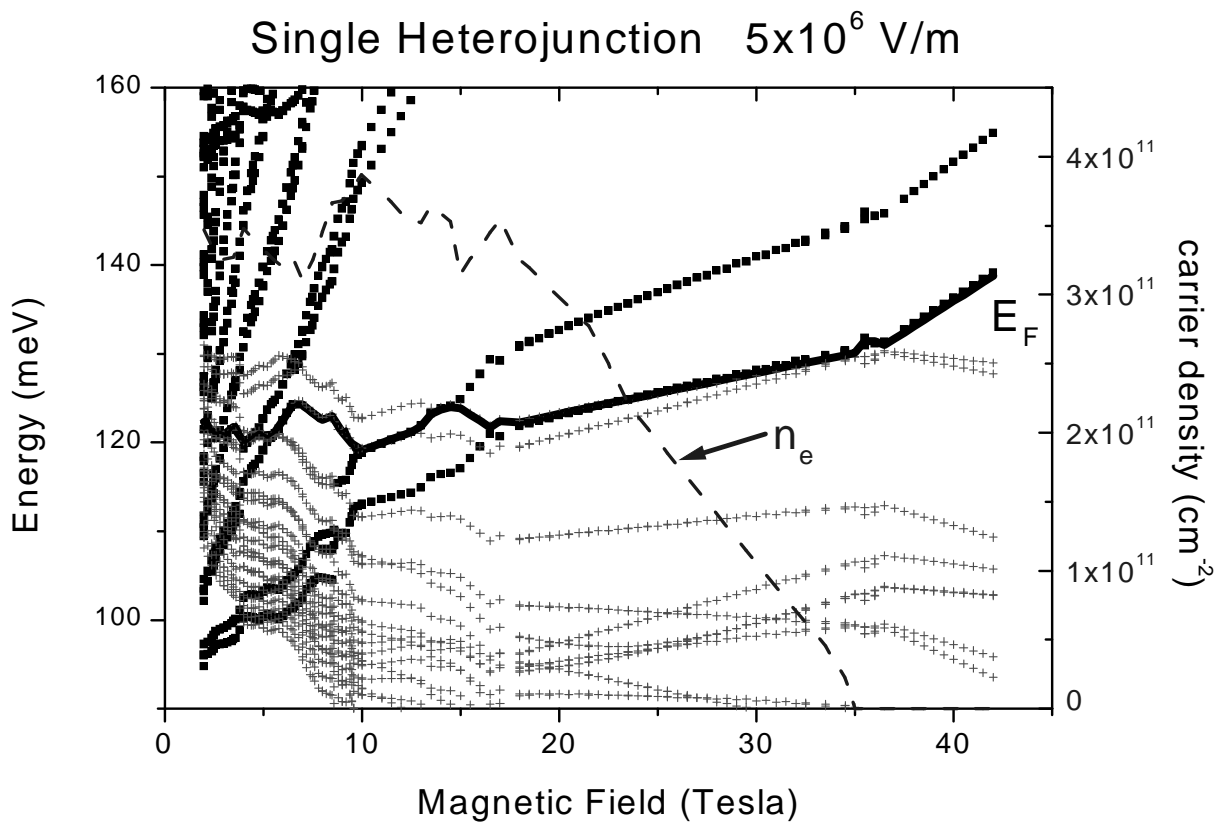


**Fig. 10**

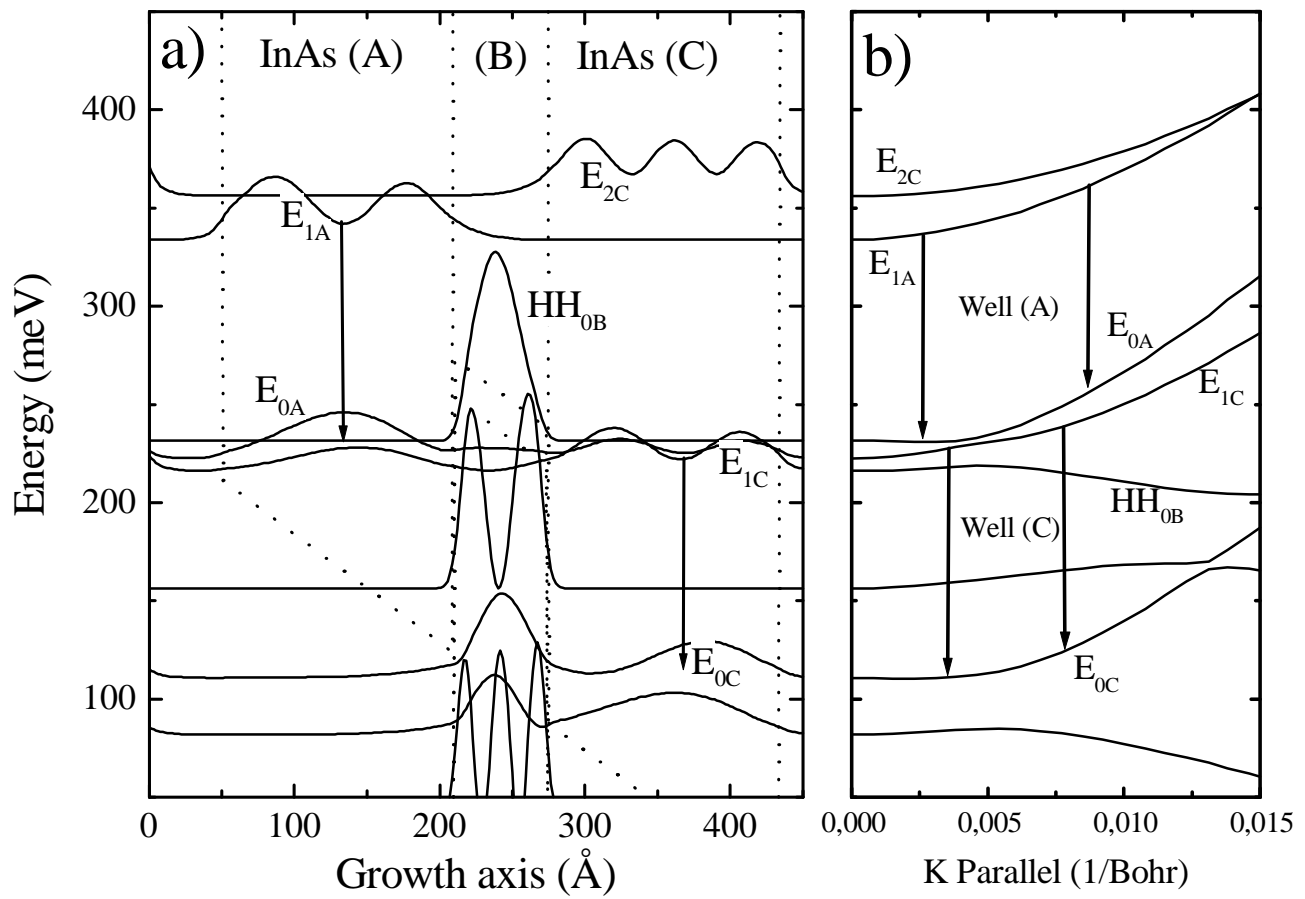


**Fig. 11**